4-2012

Synoptic-Scale Analysis of Freezing Rain Events in Montreal, Quebec, Canada

Gina M. Ressler
The Weather Network

Shawn M. Milrad
McGill University, milrads@erau.edu

Eyad H. Atallah
McGill University

John R. Gyakum
McGill University

Scholarly Commons Citation

Ressler, G. M., Milrad, S. M., Atallah, E. H., & Gyakum, J. R. (2012). Synoptic-Scale Analysis of Freezing Rain Events in Montreal, Quebec, Canada. *Weather and Forecasting, 27*(2). https://doi.org/10.1175/WAF-D-11-00071.1

Synoptic-Scale Analysis of Freezing Rain Events in Montreal, Quebec, Canada

GINA M. RESSLER,* SHAWN M. MILRAD, EYAD H. ATALLAH, AND JOHN R. GYAKUM

Department of Atmospheric and Oceanic Sciences, McGill University, Montreal, Quebec, Canada

(Manuscript received 29 June 2011, in final form 15 October 2011)

ABSTRACT

Freezing rain is a major environmental hazard that is especially common along the St. Lawrence River valley (SLRV) in southern Quebec, Canada. For large cities such as Montreal, severe events can have a devastating effect on people, property, and commerce. In this study, a composite analysis of 46 long-duration events for the period 1979–2008 is presented to identify key synoptic-scale structures and precursors of Montreal freezing rain events. Based on the observed structures of the 500-hPa heights, these events are manually partitioned into three types—west, central, and east—depending on the location and tilt of the 500-hPa trough axis. West events are characterized by a strong surface anticyclone downstream of Montreal, an inverted trough extending northward to the Great Lakes, and a quasi-stationary area of geostrophic frontogenesis located over Quebec. Central events are characterized by a cyclone–anticyclone couplet pattern, with a deeper surface trough extending into southern Ontario, and a strong stationary anticyclone over Quebec. East events are characterized by the passage of a transient well-defined cyclone, and a weaker downstream anticyclone. In all cases, cold northeasterly winds are channeled down the SLRV primarily by pressure-driven channeling. Northeasterly surface winds are associated with strong low-level temperature inversions within the SLRV. Additionally, west events tend to have a longer duration of weaker precipitation, while east events tend to have a shorter duration of more intense precipitation. The results of this study may aid forecasters in identifying and understanding the synoptic-scale structures and precursors to Montreal freezing rain events.

1. Introduction

a. Motivation

Freezing rain is one of winter's worst hazards (Dore 2003). Minor icing accumulations can make sidewalks and roads dangerously slick, while severe events can result in power outages and significant property damage. Although major freezing rain events are relatively rare (Henson and Stewart 2007), they are among the costliest of all Canadian hydrometeorological disasters (Dore 2003). A tragic reminder is the 1998 Ice Storm, when between 80 and 100 mm of freezing rain fell in the Montreal area (Milton and Bourque 1999). This unprecedented event brought down millions of trees and 120 000 km of power lines and telephone cables (Regan 1998). One million people were left without power, 100 000 people had to seek refuge in shelters, and 21 fatalities in Quebec were attributed to the event (Regan 1998; Statistics Canada 1998). Although freezing rain affects many parts of Canada, it is especially common along the St. Lawrence River valley (SLRV) in southern Quebec (MacKay and Thompson 1969; Cortinas et al. 2004). While forecasters closely monitor weather systems that may produce freezing rain, the mesoscale nature of these events makes the exact location and severity difficult to forecast (Rauber et al. 1994; Czys et al. 1996; Bourgouin 2000; Lackmann et al. 2002).

Freezing precipitation may form through two microphysical processes. The first, known as the melting process, occurs when ice crystals fall from aloft into an elevated warm (>0°C) layer of the atmosphere. After melting completely, the droplets continue to fall through a low-level subfreezing layer until they become supercooled. The supercooled droplets then freeze on contact to objects at the surface (Forbes et al. 1987; Martner et al. 1993; Czys et al. 1996). The second process, known as the supercooled warm rain process (Huffman and

* Current affiliation: The Weather Network (Pelmorex Media Inc.), Oakville, Ontario, Canada.

Corresponding author address: Gina M. Ressler, The Weather Network (Pelmorex Media Inc.), 2655 Bristol Circle, Oakville ON L6H 7W1, Canada.
E-mail: gressler@pelmorex.com

DOI: 10.1175/WAF-D-11-00071.1

Norman 1988), occurs when droplets grow by collision and coalescence, often without the presence of an elevated warm layer (Bocchieri 1980). The melting process is generally associated with the formation of freezing rain (droplets larger than 0.5 mm in diameter), while the supercooled warm rain process is associated with freezing drizzle (droplets 0.5 mm in diameter or smaller) (Rauber et al. 2000). Since these processes may occur in very different synoptic-scale environments, this study will focus only on observations of freezing rain. The SLRV is one of the only places in Canada where the occurrence of freezing rain is higher or comparable to the occurrence of freezing drizzle (Stuart and Isaac 1999).

There have been several studies on the type and frequency of synoptic-scale weather patterns associated with freezing rain. The majority of studies use a manual classification approach to examine this relationship. Bernstein et al. (1998) used a 3-yr dataset for the continental United States to investigate the locations of freezing precipitation relative to the position of surface features such as fronts, low pressure centers, and air masses of different origins. The authors found that freezing rain occurred most often in Arctic and East Coast air masses, with the highest threat values (observations per unit area) ahead of active or stationary warm fronts. Rauber et al. (2001) also used a manual classification approach to examine 411 winter storms in the United States for the time period 1970–94. They identified seven archetypal weather patterns associated with freezing precipitation events east of the Rockies. Seventy-four percent of freezing precipitation events occurred in one of four distinct surface weather patterns: (a) arctic fronts, (b) the warm front–occlusion sector of cyclones, (c) cyclone–anticyclone couplets, and (d) the west quadrant of anticyclones. Three additional patterns (East Coast cold-air damming with an anticyclone, cold-air damming with a coastal cyclone, and cold-air trapping during approaching continental cyclones) were associated with freezing precipitation in and along the Appalachian Mountains.

In recent years, many researchers have turned to automated typing procedures to classify events. Cheng et al. (2004) used principal component and discriminant function analysis to identify synoptic-scale weather patterns associated with freezing rain events in Ottawa, Ontario (CYOW). They found four surface patterns that accounted for 92% of freezing rain events lasting greater than or equal to 6 h. Each of the four types was similar in structure to one of those identified by Rauber et al. (2001), with the highest frequency of freezing rain occurring in the cyclone–anticyclone couplet pattern.

Our understanding of the synoptic-scale weather patterns associated with freezing rain events in Montreal is primarily derived from case study analyses (e.g., Higuchi et al. 2000; Gyakum and Roebber 2001; Roebber and Gyakum 2003; Henson et al. 2007). Milton and Bourque (1999) outline four components necessary for the production of freezing rain in the SLRV: (a) an airmass containing sufficient moisture, (b) the potential for meso- or synoptic-scale ascent, (c) a constant inflow of warm air aloft, and (d) a low-level layer of subfreezing air.

The conditions described by Milton and Bourque (1999) are often met by the presence of a surface cyclone over eastern Ontario or western Quebec, with the associated southerly geostrophic flow bringing warm, moist air into the Montreal region. A stationary anticyclone over Labrador or eastern Quebec will provide the cold air necessary to sustain the subfreezing layer at the surface (Milton and Bourque 1999).

These conditions are locally enhanced by the topography of the SLRV (Fig. 1) (Amante and Eakins 2009). The SLRV is oriented in a southwest–northeast direction, extending from Lake Ontario, past Montreal, to the Gulf of the St. Lawrence near the Gaspé Peninsula. In certain situations where there is higher pressure to the northeast of Montreal and lower pressure to the southwest (such as the conditions described above), a strong pressure gradient force (PGF) is induced along the valley. If the PGF is strong enough, winds within the SLRV will become channeled down the valley toward lower pressure, even when the geostrophic wind is directed perpendicular to the valley axis. This type of pattern, known as pressure-driven channeling, is the dominant mechanism for producing northeasterly surface winds at Montreal (Carrera et al. 2009; Razy et al. 2012). Stuart and Isaac (1999) found that almost all occurrences of freezing precipitation at Montreal are reported with northeasterly surface winds. Furthermore, Roebber and Gyakum (2003) showed that during the 1998 Ice Storm a frontogenetic focus was provided by the pressure-driven channeling of cold northeasterly surface winds with warm geostrophic southerlies. They found that this valley-enhanced frontogenesis was a fundamental contributor to higher precipitation amounts during the event. Using model sensitivity estimates, Roebber and Gyakum (2003) showed that, in the absence of the SLRV topography, total freezing rain volumes in the Montreal area would have been reduced by 12.1% and 16.5% in the first and second precipitation episodes, respectively.

b. Objectives

Much of the previous work done on freezing rain has focused on one of three areas: analyzing the climatology (e.g., Laflamme and Periard 1998; Stuart and Isaac 1999; Cortinas et al. 2004), conducting individual case studies (e.g., Forbes et al. 1987; Rauber et al. 1994; Gyakum and

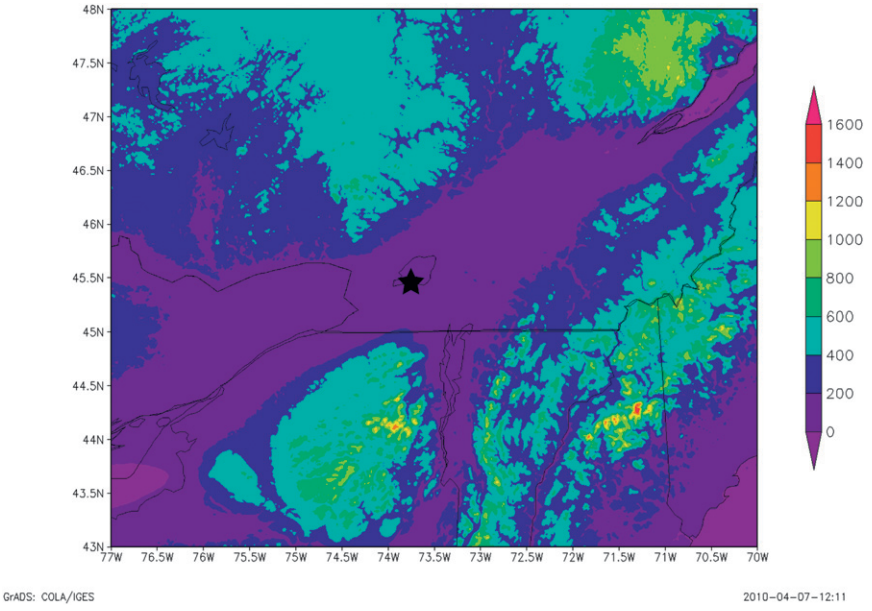

FIG. 1. Elevation map of the SLRV, plotted using the Elevation Data for Areas Greater than 1 Arc-Minute (ETOP1) Global Relief Model (Amante and Eakins 2009). Scale shown in m. The star represents the location of Montreal (CYUL).

Roebber 2001), or developing statistical methods to improve prediction (e.g., Bocchieri 1980; Czys et al. 1996; Bourgouin 2000). Few studies have conducted a thorough synoptic-scale analysis of freezing rain events in Canada, fewer still in Quebec.

Given the hazardous nature of freezing rain within the SLRV and the importance of accurate forecasts, more work is needed to understand the atmospheric environments and precursors associated with these events. Roebber and Gyakum (2003) point out that the mesoscale processes that lead to freezing rain at Montreal are often controlled by the synoptic-scale pressure fields. Therefore, the main objective of this study is to examine and document the pertinent synoptic-scale features preceding typical freezing rain events in Montreal. This is achieved by performing a manual synoptic typing of the most severe events reported in the time period 1979–2008. The synoptic-scale dynamics of each type of freezing rain event are examined, as well as moisture fields, precipitation rates, and total accumulations. One goal of this study is to equip the local forecaster with the ability to recognize each type of freezing rain event, providing further insight into event causation, evolution, and severity, and helping to improve freezing rain predictions in the SLRV.

The outline of the paper is as follows. Section 2 describes the data and methodology. In section 3, the composite results and precipitation analysis are presented. A concluding discussion is given in section 4.

2. Data and methodology

a. Data

Hourly surface observations for the Pierre Elliott Trudeau International Airport (CYUL), located in Montreal (Dorval), Quebec, are retrieved from Environment Canada's Digital Archive of Canadian Climatological Data for seven winter months (October–April) for the period 1979–2008. Environment Canada 6-hourly total precipitation values at CYUL for the same time period are obtained through the Data Access Integration (DAI) online catalogue [available at http://loki.qc.ec.gc.ca/DAI/; DAI (2010)].

The time period 1979–2008 is chosen because of the availability of the National Centers for Environmental Prediction (NCEP) North American Regional Reanalysis (NARR) dataset (Mesinger et al. 2006). The NARR is a long-term, high-resolution dataset for the study of climate- and hydrological-related phenomena. The NARR incorporates a version of the NCEP North American Mesoscale (NAM) model, with 32-km resolution, 45 vertical layers, and with analyses performed every 3 h. The majority of the calculations and analyses in this study are performed and displayed using the General Meteorological Package, version 5.7.11 (Koch et al. 1983).

b. Definition of events

Using Environment Canada hourly surface observations, we identify 200 incidents of continuous or near-continuous

freezing rain at CYUL. ''Near continuous'' in this context means that there were fewer than six consecutive hours of nonfreezing rain observations between every hour of freezing rain. Continuous in this context means that there were no nonfreezing rain observations between freezing rain observations. Of these incidents, 163 are considered to be synoptically independent, defined as having at least 3 days of nonfreezing rain observations between each event.

The hourly surface observations for the period 1979–2008 indicate that CYUL receives approximately 28 hours of freezing rain per year. All freezing rain observations for the period 1979–2008 occurred between November and April, with the highest frequency reported in December (8.73 h yr^{-1}) and January (7.23 h yr^{-1}). At certain airports, including CYUL, freezing rain is also measured for its rate of fall on an hourly basis. The rate of fall is categorized as light (<2.5 mm h^{-1}), moderate (2.5–7.5 mm h^{-1}), or heavy (>7.5 mm h^{-1}). For the time period of 1979–2008, light intensity is reported for 98% of all freezing rain observations (835 out of 850 reports).

Theoretically, event severity should be derived from a measure of the total ice accumulation. However, contrary to rain and snow, no direct measurement of freezing rain accumulation is made in Canada. Freezing rain accumulation is included in the liquid accumulation totals. Therefore, freezing rain amounts are typically inferred from the rain rate. In this study, since the predominant intensity of freezing rain is light, only the number of freezing rain hours per event is used to define the severity. The event duration is defined as the number of hours from the first freezing rain report to the last, with the possibility of nonfreezing rain observations in between.

Freezing rain events at CYUL are typically short lived. The distribution of freezing rain hours per event, illustrated in Fig. 2, shows that as the number of hours increases, the frequency decreases exponentially. The median value of freezing rain hours per event is three. One can speculate on the reasons behind the short-lived nature of freezing rain events. Warm-air advection at the surface may be a limiting factor, since many freezing rain events are associated with the passage of a warm front (Bernstein et al. 1998; Rauber et al. 2001). When horizontal advection is weak, Stewart (1985) suggests that latent heat exchange may contribute to the short-lived nature of freezing rain. As ice crystals aloft fall through an elevated warm layer, they melt, absorbing latent heat and cooling the surrounding environment. In the absence of thermal advection, the continued melting of ice crystals will eventually cool the warm layer to 0°C. Similarly, the refreezing of supercooled water droplets at the surface will release latent heat, warming the cold layer to 0°C. This process will eventually destroy the temperature inversion, and the freezing rain will change to another form of precipitation (Stewart 1985; Kain et al. 2000).

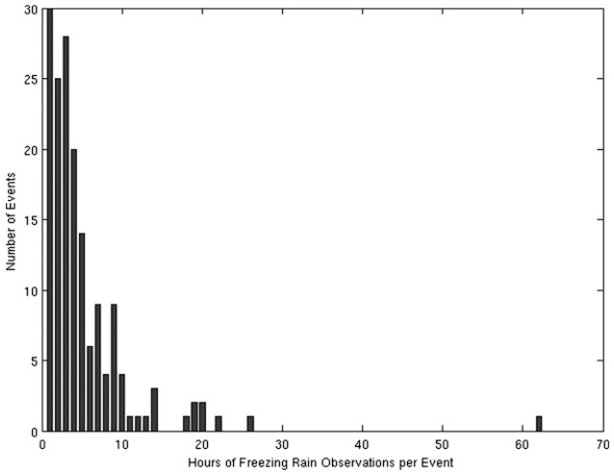

FIG. 2. Histogram of freezing rain hours per event.

Seventy-five percent of all events have less than 6 h of freezing rain. Therefore, in this study, we define long-duration events as having ≥6 h of freezing rain observations per event. Cortinas (2000) and Cheng et al. (2004) also used a 6-h threshold to define long-duration freezing rain events in the Great Lakes region and Ottawa areas, respectively. By this definition, there are 46 long-duration events at CYUL during the period 1979–2008. The event onset time (hereafter denoted as $t = 0$ h) is defined as the time of the first freezing rain observation for each event. For events with discontinuous freezing rain (more than six consecutive hours of nonfreezing rain observations between freezing rain observations), the onset time is defined as the start time of the long-duration freezing rain (≥6 h of continuous freezing rain). In the composite analysis, onset times are rounded to the nearest 3-h interval to correspond to the time steps used in the NARR dataset.

c. *Manual synoptic partitioning*

For each long-duration event, the 500-hPa heights, 500-hPa vorticity, and sea level pressure (SLP) fields are examined. Based on the observed structures of the 500-hPa heights, a manual synoptic typing is used to partition events into three types—west, central and east—depending on the location and tilt of the long-wave 500-hPa trough over North America at $t = 0$ h (Fig. 3). Partitioning the events in this way will ensure that the large-scale processes controlling the environment are consistent within each type. Large-scale features can also provide insight into the dynamics driving

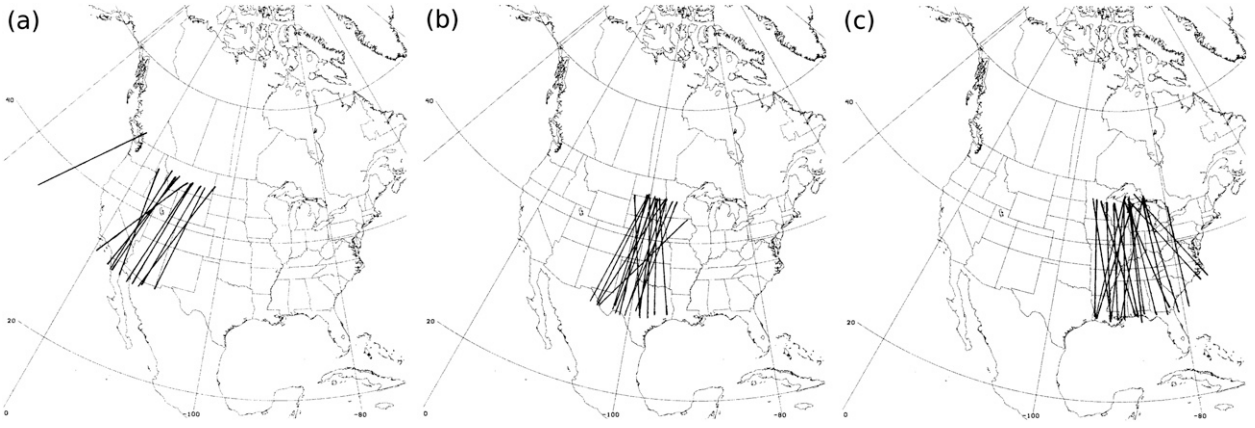

FIG. 3. The location and orientation of the 500-hPa trough axis at $t = 0$ h for each (a) west, (b) central, and (c) east long-duration event.

the surface features, different mechanisms for vertical motion, and the speed at which features move across the continent. Additionally, differences in the large-scale structure of the environment may have implications on the predictability of certain types of events.

The main partitioning criterion is the location of the long-wave 500-hPa trough axis. West events ($n = 10$) are characterized by a long-wave trough over the western third of the United States (west of the Front Range of the Rocky Mountains) (Fig. 3a). Central events ($n = 16$) are characterized by a long-wave trough over the central United States (Fig. 3b), with a ridge already building over the west coast. Ridging over the West Coast is not present in any of the west events. East events ($n = 20$) are characterized by a long-wave trough east of approximately 95°W (Fig. 3c). The 95°W line is chosen since the majority of the trough axes to the west of 95°W are positively tilted, and the majority of the trough axes to the east of 95°W are neutrally or negatively tilted. Events that have a trough axis located near 95°W are partitioned based on the tilt of the axis. Events that have a long-wave trough axis with a neutral or negative tilt near 95°W are considered east events, and events that have a long-wave trough axis with a positive tilt are considered central events. The tilt of the trough is used as a tiebreaker between east and central events since all clear-cut east events have a negatively tilted trough (Fig. 3c), and all clear-cut central events have a positively tilted trough (Fig. 3b). No tiebreaker is required for west and central events (Figs. 3a,b). Short-wave vorticity maxima are not considered when partitioning events.

The primary weakness of manual synoptic typing is the inherent subjectivity of the method. There is also the question of whether the partitioning is repeatable or not. In this study, the partitioning criteria have been made as objective as possible, while still relying on an understanding of upper-level atmospheric dynamics. Although a small number of cases could be classified as either central or east by an objective observer, the choice of synoptic type for these few cases does not significantly impact the results.

To visualize the mean and spread of each synoptic type, spaghetti plots are shown in Fig. 4 for the 558-dam contour of the 500-hPa pressure level. Central events show the most variability, and this suggests that more smearing will impact this category's composite diagnostics discussed in section 3.

3. Results

a. Duration and severity

For each synoptic type, the median duration and number of hours of freezing rain per event are calculated at CYUL. The event duration is defined as the number of hours from the first freezing rain observation to the last, with the possibility of nonfreezing rain observations in between. The number of freezing rain hours is defined as the number of reports of freezing rain within the event duration. The number of freezing rain hours is used as a proxy for the severity of each event. On average, west events have the longest duration (median 25.5 h), with the most hours of freezing rain per event (median 11.5 h). East events have the shortest duration (median 12.0 h), with the fewest number of hours of freezing rain per event (median 8.5 h). Table 1 displays the median values of duration and freezing rain hours for all three types. Median values are displayed instead of mean values, since the distribution of each variable is positively skewed (Fig. 2). On average, west events last more than twice as long as east events. The results of the duration statistics will be discussed in more detail in the next section, in conjunction with the composite analysis.

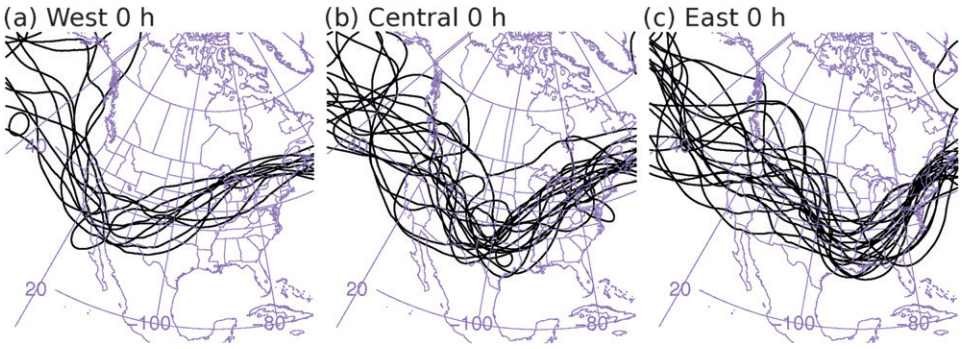

FIG. 4. Spaghetti plot of the 558-dam contour of the 500-hPa pressure level at $t = 0$ h for each (a) west, (b) central, and (c) east long-duration event.

b. Composite results

The composite dynamics in this study will be examined from a quasigeostrophic (QG) perspective. Since the production of freezing rain requires warm air advection (WAA) and rising motion (Milton and Bourque 1999), we examine the processes associated with QG forcing for ascent (Bluestein 1992, p. 328): differential cyclonic vorticity advection (CVA) and WAA. These processes are represented by the two terms on the right-hand side of the adiabatic, frictionless form of the QG omega equation:

$$\left(\nabla_p^2 + \frac{f_0^2}{\sigma}\frac{\partial^2}{\partial p^2}\right)\omega = -\frac{f_0}{\sigma}\frac{\partial}{\partial p}[-\mathbf{v}_g \cdot \nabla_p(\zeta_g + f)] + \frac{R}{\sigma p}[-\nabla_p^2(-\mathbf{v}_g \cdot \nabla_p T)], \quad (1)$$

where f and σ are the Coriolis and static stability parameters, ζ_g and $\mathbf{v}_g$ are the geostrophic relative vorticity and the geostrophic wind, R is the gas constant, p is pressure, and T is temperature.

To identify synoptic-scale features and precursors, composite fields are displayed for each type at $t = -48$, -24, and 0 h (frontogenesis fields are displayed at $t = 0$, $+12$, and $+24$ h). Anomaly fields are defined as a departure from monthly weighted climatological values, which are computed using 30-yr averages for the period 1971–2000. The statistical significance of the anomalies is evaluated using the Student's t test [see Eq. (5.3) on p. 139 of Wilks (2006)]:

$$t_{\text{dis}} = \frac{\overline{x} - \mu_0}{[\widehat{\text{var}}(\overline{x})]^{1/2}}, \quad (2)$$

where t_{dis} is the distribution, $\overline{x}$ is the observed sample mean, μ_0 is the population mean, and the denominator is the square root of the variance of the sample mean.

Figure 5 illustrates the 500-hPa height and absolute vorticity composite fields for each synoptic type at $t = 0$ h, the start time of freezing rain. The partitioning criteria are reflected in the location and tilt of the composite trough axis. West and central events are characterized by a positively tilted trough with vorticity maxima located over the west and central regions of the United States, respectively. East events are characterized by a negatively tilted trough, and stronger values of absolute vorticity located just south of the Great Lakes. The wavelength of the 500-hPa height field is shortest in the east composite (Fig. 5c) and longest in the west composite (Fig. 5a). The half-wavelengths are approximately 1500 and 3000 km for the east and west composites, respectively. Since shorter wavelengths are accompanied by faster eastward movement, we expect the troughs and associated surface features in the east events to move through the CYUL region more quickly. The hourly observations support this, since east events last, on average, only half as long as west events (Table 1).

The 1000–500-hPa thickness fields for all three types at $t = -48$ h show statistically significant cold anomalies over the west coast of the United States (Figs. 6a–c), indicative of the advancing upper-level trough. The west and central composites also show the advection of cold arctic air throughout Quebec 48 h before the onset of freezing rain. The west composite (Fig. 6a) already shows a statistically significant warm anomaly of $+12$ dam over the central plains of the United States. This warm signal is not yet present in the central or east composites.

TABLE 1. Median number of freezing rain hours and freezing rain duration, calculated from Environment Canada hourly observations at CYUL.

Variable	West	Central	East
Total number of events (n)	10	16	20
Median freezing rain hours (h)	11.5	9	8.5
Median duration (h)	25.5	12.5	12

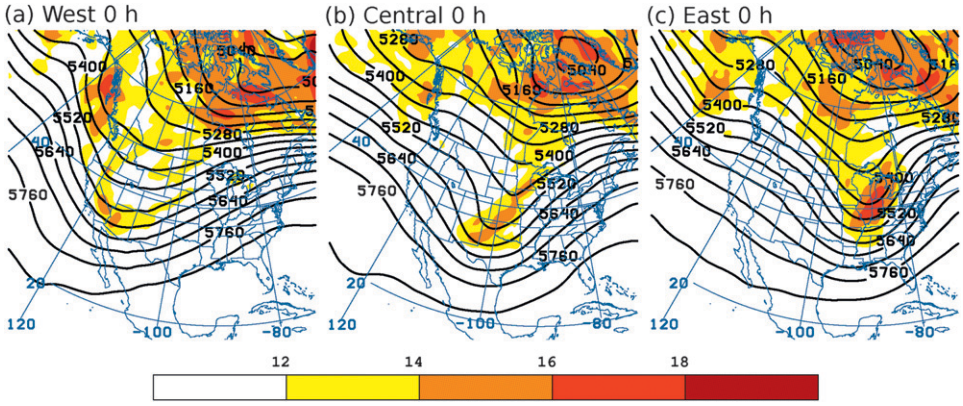

FIG. 5. Composite plots of 500-hPa geopotential height (solid, m) and absolute vorticity (shaded, 10^{-5} s^{-1}) at $t = 0$ h for (a) west, (b) central, and (c) east events.

The WAA in the 1000–500-hPa layer of the west composite builds the upper-level ridge over the eastern half of North America (Fig. 5a). Advection of anticyclonic vorticity downstream of the 500-hPa ridge (QG forcing for descent) is associated with upper-level convergence and the development of a surface anticyclone over Quebec and the Maritime Provinces (Fig. 6g). The central and east composites do not show statistically significant warm anomalies until $t = -24$ h (Figs. 6e,f). These features strengthen as they migrate eastward, so that by $t = 0$ h, all three composites show statistically significant warm thickness anomalies over southern Ontario and Quebec (Figs. 6g–i). The west composite shows the most impressive warm anomaly, with a value of +18 dam. This corresponds to an anomaly of +9°C in the mean temperature of the 1000–500-hPa layer, using the hypsometric equation (Bluestein 1992, p. 58). Consequently, the west composite shows higher 500-hPa heights over CYUL at the time of freezing rain onset (Fig. 5a), as well as the broadest downstream anticyclone (Fig. 6g). All three composites indicate 1000–500-hPa WAA into the CYUL region at the time of freezing rain onset.

It should also be noted that the west and, to a lesser extent, central composites show strong cold-air advection (CAA) and an anomalous cold pool of air over northern Quebec, Newfoundland, and Labrador in the 48 h leading up to freezing rain onset (Figs. 6a,d,g and Figs. 6b,e,h). This suggests that more cold air is available in west events to sustain the low-level temperature inversion. In the east composite, while CAA is present over Newfoundland and Labrador, the cold thickness anomalies are weaker and displaced farther north, over Baffin Island (Figs. 6c,f,i). This suggests that the cold pool is weaker in east events, leading to weaker low-level temperature inversions and shorter-lived events.

The composite plots of SLP at $t = 0$ h indicate a strong PGF aligned with the axis of the SLRV for all three types (Figs. 6g–i). Given the strength and orientation of the PGF, we would expect cold northeasterly surface winds at CYUL at the onset time of freezing rain. The east composite (Fig. 6i) shows a well-defined surface cyclone located downstream from the 500-hPa trough axis (Fig. 5c), with a value of 1004 hPa in the lowest contour. The west and central composites show weaker low pressure centers of 1012 hPa (Figs. 6g,h). The west and central composites do, however, have stronger high pressure systems to the northeast, contributing to the strong PGF along the SLRV.

To a first approximation, all three SLP composites are similar to the cyclone–anticyclone couplet pattern documented by Rauber et al. (2001) (type C), Cheng et al. (2004) (type 2), and Milton and Bourque (1999). However, there are a few important details that distinguish each synoptic type. The stronger anticyclone in the west and central SLP composites bears resemblance to the surface pattern of type D (western quadrant of anticyclones) from Rauber et al. (2001). In fact, an individual examination of all 10 west events reveals that 9 have no well-defined cyclone at all (Fig. 7a). The cyclone in the east SLP composite shows similarities to the surface pattern of type B (warm front–occlusion sector of cyclones) from Rauber et al. (2001), as well as to types 1 and 3 from Cheng et al. (2004). Similarly, a small number of east events have a distinct lack of a downstream anticyclone (Fig. 8c). This implies that although a strong pressure gradient is needed along the SLRV to induce northeasterly channeled winds, this can be accomplished by a cyclone or anticyclone alone, not necessarily both.

Although the surface winds are northeasterly, the surface geostrophic winds from the composite plots of SLP are southwesterly, southerly, and southeasterly over CYUL, for the west, central, and east composites, respectively. This provides further proof that pressure-driven channeling is a critical mechanism for the production of

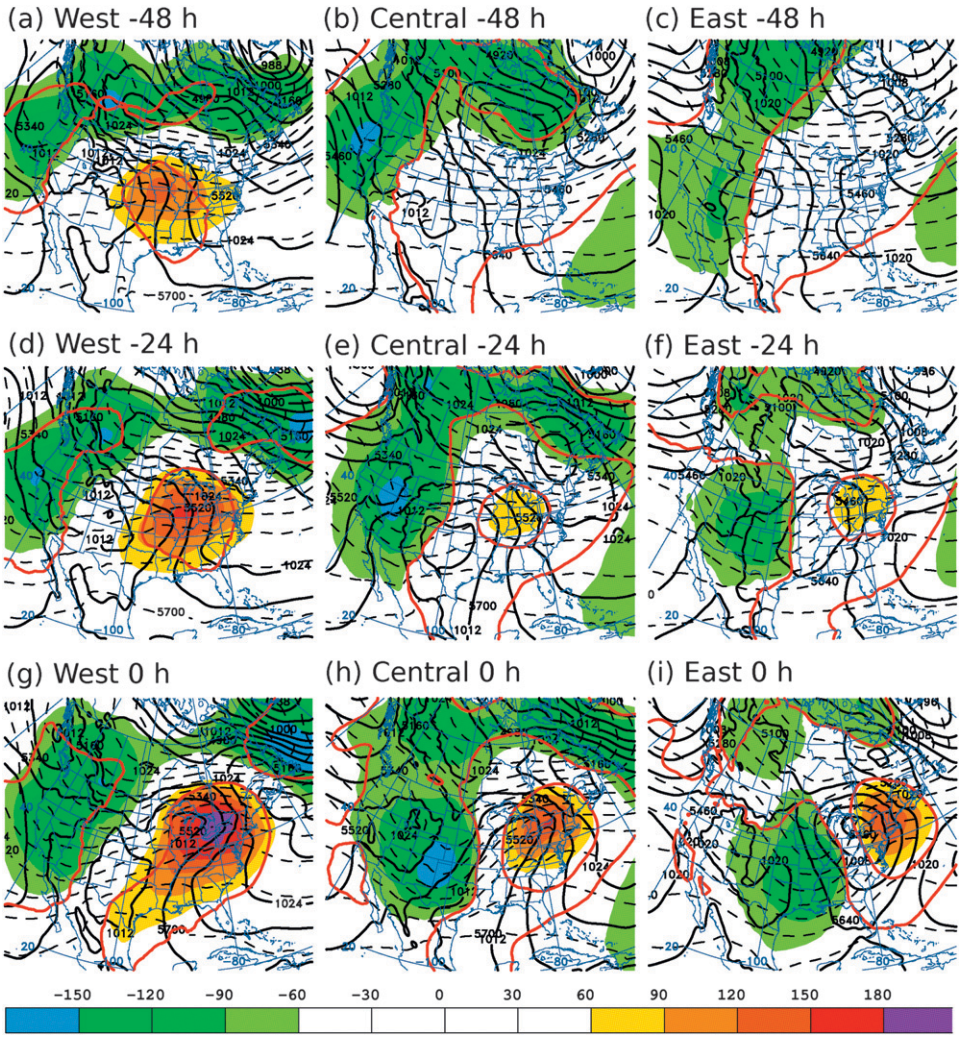

FIG. 6. Composite 1000–500-hPa thickness (dashed, interval of 60 m), thickness anomalies (shaded, interval of 30 m) with respect to climatology, and composite SLP (solid, 4-hPa interval) at $t = -48, -24$, and 0 h for (a),(d),(e) west, (b),(e),(h) central, and (c),(f),(i) east events. The solid red contour represents the statistical significance of the thickness anomalies at the 99% confidence level, according to the Student's t test.

freezing rain in CYUL (Carrera et al. 2009; Razy et al. 2012).

One drawback of using the QG omega equation [Eq. (1)] is that the two forcing terms on the right-hand side may act in opposition to each other. Therefore, it is often helpful to explicitly diagnose regions of forcing for ascent using the **Q**-vector representation of the QG omega equation, which combines the two terms on the right-hand side of Eq. (1) (Hoskins et al. 1978). The **Q**-vector representation of the QG omega equation may be expressed as

$$\left(\nabla_p^2 + \frac{f_0^2}{\sigma}\frac{\partial^2}{\partial p^2}\right)\omega = -2\nabla_p \cdot \mathbf{Q}, \tag{3}$$

where

$$\mathbf{Q} = -\frac{R}{\sigma p}\begin{pmatrix} \dfrac{\partial \mathbf{v}_g}{\partial x}\cdot\nabla_p T \\ \dfrac{\partial \mathbf{v}_g}{\partial y}\cdot\nabla_p T \end{pmatrix} = \begin{pmatrix} Q_1 \\ Q_2 \end{pmatrix} \tag{4}$$

if the Coriolis parameter, f, is assumed to be constant.

The forcing of ω is proportional to the horizontal divergence of the **Q** vector (in the midtroposphere):

$\nabla_p \cdot \mathbf{Q} > 0 \rightarrow \omega > 0$ (forcing for sinking motion) and

$\nabla_p \cdot \mathbf{Q} < 0 \rightarrow \omega < 0$ (forcing for rising motion).

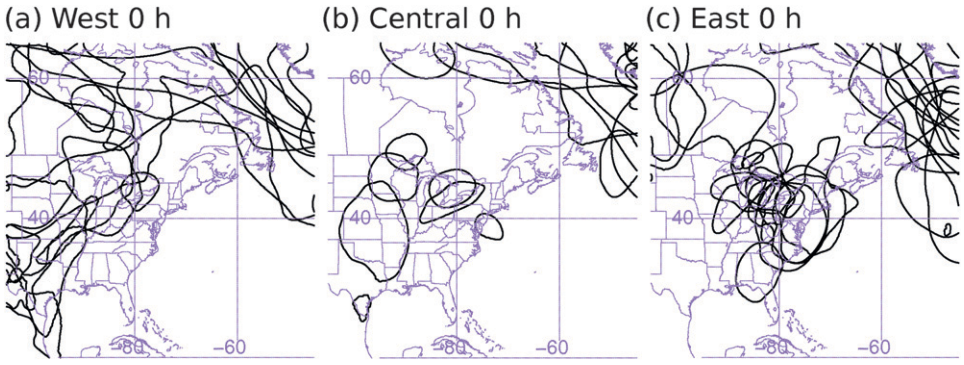

FIG. 7. Spaghetti plot of the 1008-hPa contour of SLP at $t = 0$ h for each (a) west long-duration event and the 1000-hPa contour of SLP at $t = 0$ h for each (b) central and (c) east long-duration event.

Figure 9 shows the locations of **Q**-vector convergence, calculated from the 700-hPa composite wind and temperature fields at $t = 0$ h. All three composites show forcing for ascent in the CYUL region at the time of freezing rain onset. The area of **Q**-vector convergence in the west composite is elongated along the Ottawa and St. Lawrence River valleys, perpendicular to the direction of WAA (Fig. 9a). The elongated area is present in the west composite from 6 h before to 6 h after freezing rain onset (not shown). This elongated area of forcing for ascent suggests the formation of a frontal zone, similar to that of the 1998 Ice Storm (Roebber and Gyakum 2003). In the east composite, there is a branch of **Q**-vector convergence to the south of CYUL, where one would expect a surface cold front (Fig. 9c). In terms of duration, in the central and east composites, the area of **Q**-vector convergence is displaced northeast of CYUL by $t = +6$ h (not shown). Therefore, the duration of forcing for ascent in the CYUL region lasts the longest in the west composite. All three composites show high (>80%) values of relative humidity in the freezing rain region (Figs. 9a–c).

The time evolution of the 250-hPa jet structure is shown in Fig. 10. The west composite (Fig. 10a) shows a well-defined jet streak over Quebec oriented zonally, 48 h before the onset of freezing rain. The location of the jet streak corresponds to the strong temperature gradient present in the 1000–500-hPa thickness field at $t = -48$ h (Fig. 6a). The east and central 1000–500-hPa thickness composites show weaker temperature gradients at $t = -48$ h (Figs. 6b,c) and, thus, show weaker jet streaks at 250 hPa. By $t = 0$ h, the west composite shows an enhanced zonal jet over Quebec, while the jet in the east composite is oriented meridionally (Figs. 10g–i). The meridional structure of the jet in the east composite reinforces the high-amplitude, short-wavelength nature of such events. Additionally, CVA in the equatorward entrance and poleward exit regions is associated with enhanced ascent (Bluestein 1992, p. 398). CYUL is located in the equatorward entrance region of the jet in the west and central composites (Figs. 10g,h). In the east composite (Fig. 10i), CYUL is located in the equatorward entrance region of the downstream jet and in the poleward exit region of the upstream jet. It should also be noted that the jet kinetic energy in all three composites is downstream of the upper-level trough axis. Kinetic energy associated with a jet streak downstream of the upper-level trough is often indicative of a weakening trough.

The synoptic-scale circulation features can now be related to composites of precipitable water and water vapor transport. The columnar precipitable water w is defined by

$$w = \frac{1}{gp}\int_{300\text{hPa}}^{\text{surface}} q\, dp, \tag{5}$$

where g is the gravitational constant, ρ is the density of liquid water, q is the specific humidity, and p is the pressure. We define the vertical integral of the water vapor transport vector $\mathbf{Q}_w$ as

$$\mathbf{Q}_w = \frac{1}{g}\int_{300\text{hPa}}^{\text{surface}} q\mathbf{v}\, dp, \tag{6}$$

where $\mathbf{v}$ is the horizontal wind vector.

Figure 11 shows composite and anomaly values of precipitable water (PW), as well as column-integrated water vapor transport. The west composite shows a plume of high PW values extending from the Gulf of Mexico at $t = -48$ h, through the Ohio Valley, and into the Great Lakes region by $t = 0$ h (Figs. 11a,d,g). The central composite shows a plume of moisture, similar to the west composite, but with the highest PW values displaced eastward (Figs. 11b,e,h). The east composite shows one

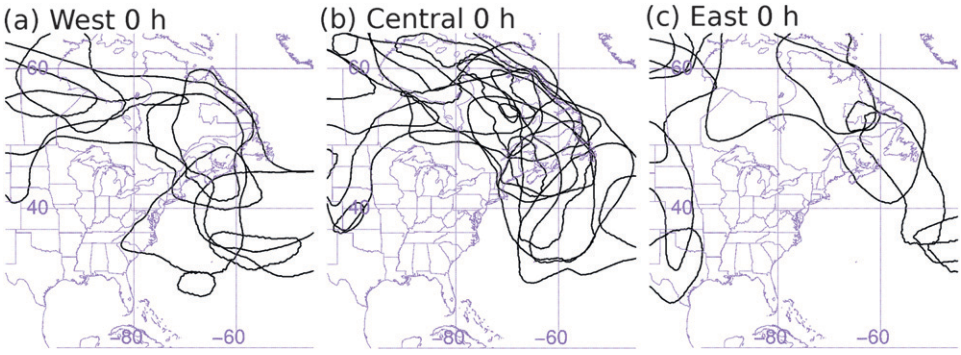

FIG. 8. As in Fig. 7, but for the 1032-hPa contour of SLP.

plume of high PW values extending from the subtropical Atlantic along the east coast of the United States (Figs. 11c,f,i). PW values at CYUL for the east and central composites at $t = 0$ h correspond to positive anomalies of approximately 10–15 mm compared to climatology. PW values for the west composite correspond to positive anomalies of approximately 5–10 mm compared to climatology. The moisture transport suggests that the Gulf of Mexico is the dominant moisture source for west and central cases. At $t = +24$ h, high PW anomalies are still present over CYUL in the west composite (not shown), while in the central and east composites, they have moved eastward out of the CYUL region. The moisture transport trajectories suggest that the Atlantic is the dominant moisture source for the east cases.

The 1000–850-hPa frontogenesis results at $t = 0$, +12, and +24 h are plotted in Fig. 12. All three composites show enhanced frontogenesis along the SLRV at $t = 0$ h, as southerly geostrophic winds, combined with channeled surface winds from the northeast, form an area of low-level frontogenesis along the valley. The frontogenesis is strong in all three types and even extends into the Ottawa River valley to the west of CYUL in the west and central composites (Figs. 12a,b). Note that the frontogenesis along both valleys corresponds to the locations of **Q**-vector convergence in Fig. 9. Also, the isobars in all three composites at $t = 0$ h show kinks near the SLRV, indicative of a frontal boundary. At $t = +12$ h, the west and central composites show stronger frontogenesis along the SLRV than does the east composite, although with a weaker signal than at $t = 0$ h (Figs. 12d–f). By $t = +24$ h, valley-enhanced frontogenesis is still present in the west composite, even though the composite surface cyclone is no longer distinguishable (Fig. 12g). A weak cyclone and weak frontogenesis are present in the central composite (Fig. 12h), but any substantial frontogenesis [greater than 0.5 K $(100\ \text{km})^{-1}$ $(3\ \text{h})^{-1}$] in the east composite is no longer present at $t = +24$ h (Fig. 12i). In the east composite at $t = +24$ h, the surface cyclone center has already passed CYUL and CAA is present in the region. At this time, freezing rain has stopped in almost all 20 east cases. Figure 12 suggests that valley-enhanced frontogenesis plays a key role in prolonging the duration of west and central events.

c. *Precipitation analysis*

The precipitation analysis in this study is limited by the amount of freezing rain data available. Recall that

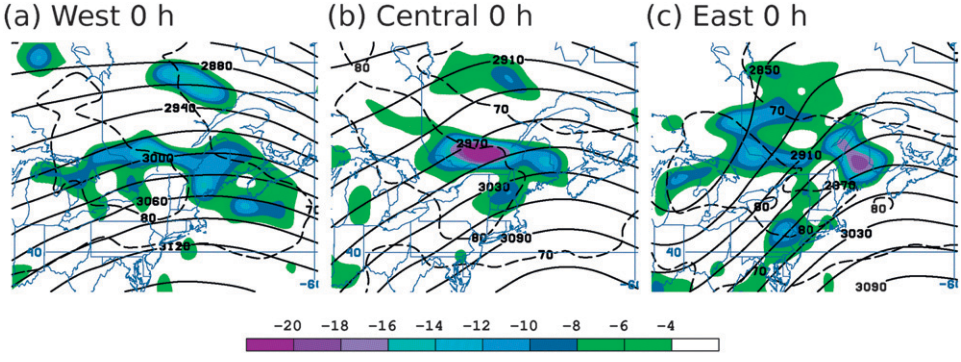

FIG. 9. Composite 700-hPa height (black solid, 30-m interval), **Q**-vector convergence (shaded, 10^{-16} K m^{-2} s^{-1}), and 1000–500-hPa relative humidity (dashed, %) at $t = 0$ h for (a) west, (b) central, and (c) east events.

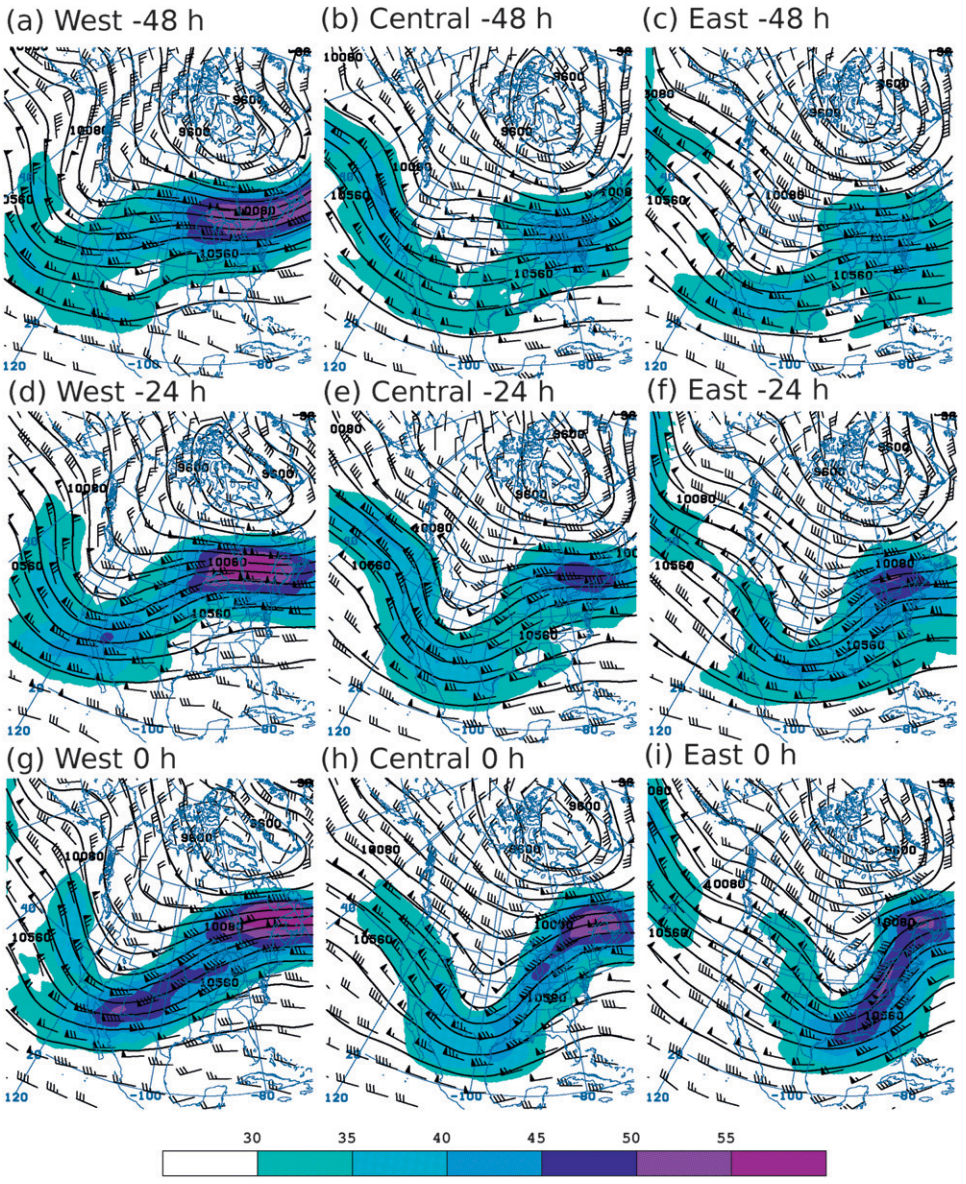

FIG. 10. Composite 250-hPa heights (solid, 120-m interval), isotachs (shaded, 5 m s^{-1} interval) and wind barbs (barb represents 5 m s^{-1}; flag represents 25 m s^{-1}) at $t = -48$, -24, and 0 h for (a),(d),(g) west, (b),(e),(h) central, and (c),(f),(i) east events.

in Canada, no direct measurement of icing accumulation is made; freezing rain is simply included in the liquid precipitation totals. Additionally, no hourly precipitation accumulations are available in Canada, regardless of type. To study the precipitation, we must use 6-hourly solid, liquid, or total precipitation accumulations. Since we cannot distinguish between freezing rain accumulation and other liquid precipitation accumulation within the 6-hourly precipitation data, we examine only the total (solid and liquid) accumulation, to facilitate the precipitation analysis.

Environment Canada 6-hourly data at CYUL are used to calculate the total (solid, liquid, and freezing) precipitation accumulation for each long-duration event. New start and end times for the entire length of the precipitation duration must be defined, since other forms of precipitation, such as rain or snow, may begin before the freezing rain, and continue after the freezing rain has finished. We define the precipitation duration as the length of time, encompassing the freezing rain observations, during which there is continuous measurable precipitation. We are then able to calculate an estimated

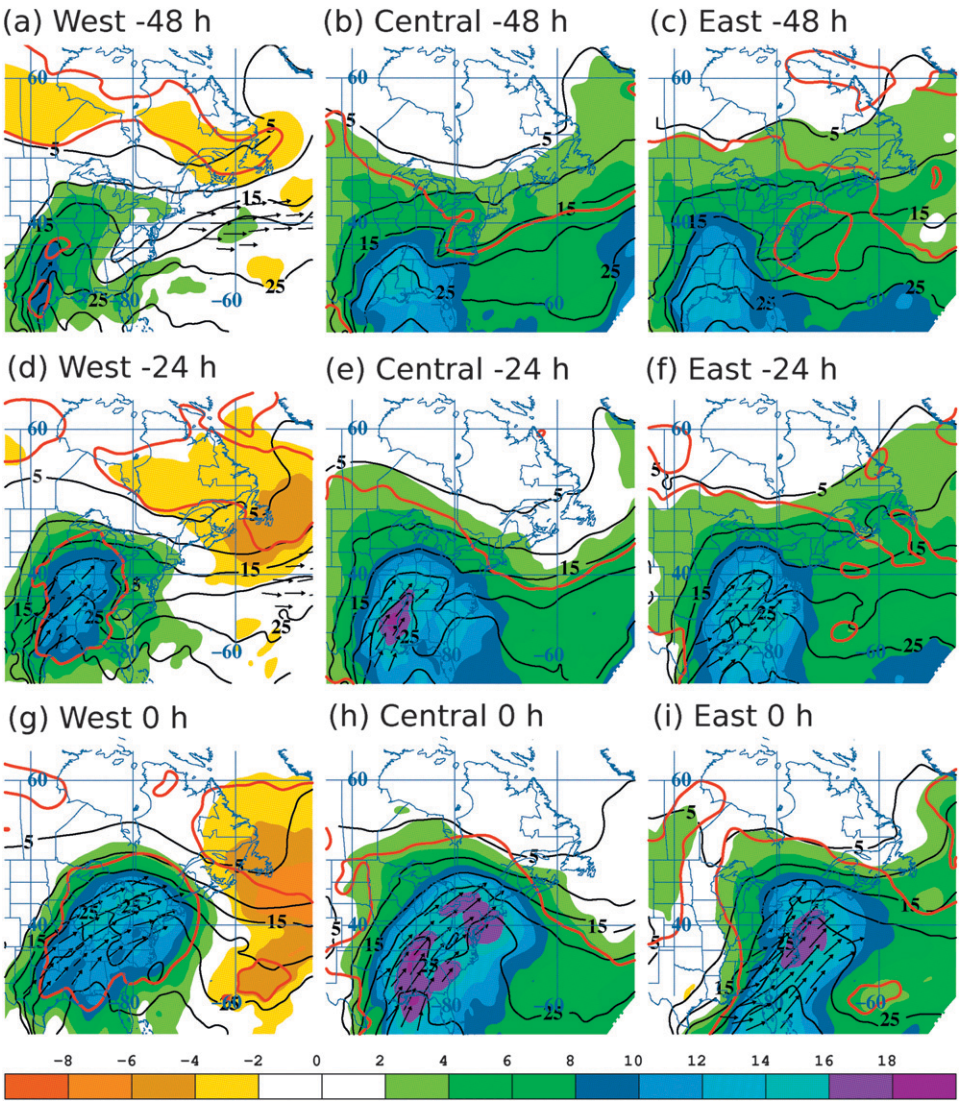

FIG. 11. Composite PW (solid, 5-mm interval), PW anomalies (shaded, mm), and water vapor transport (arrows, kg m^{-1} s^{-1}) at $t = -48$, -24, and 0 h for (a),(d),(g) west, (b),(e),(h) central, and (c),(f),(i) east events. Vectors below 5 kg m^{-1} s^{-1} are not shown. The solid red contour represents the statistical significance of the PW anomalies at the 99% confidence level, according to the Student's *t* test.

precipitation rate for each event by dividing the total accumulation by the precipitation duration. The median and maximum precipitation rates are displayed in Table 2.

In Table 1, we showed that west events had the longest duration of freezing rain. Table 2 indicates that west events also have the longest duration of total precipitation, regardless of type. However, west events are also characterized by the weakest precipitation rates, and east events are characterized by the strongest precipitation rates. Consequently, the total accumulations (liquid equivalent) are comparable across all three types, with median values between 21 and 24 mm per event. It should be noted that there is a high degree of variability between types as well as within each type. The event with the largest precipitation accumulation is the 1998 Ice Storm (a west event), which reported 99.2 mm of precipitation over a 5-day period, most of which fell as freezing rain.

4. Concluding discussion and future work

Freezing rain is a major environmental hazard for communities along the St. Lawrence River valley (SLRV),

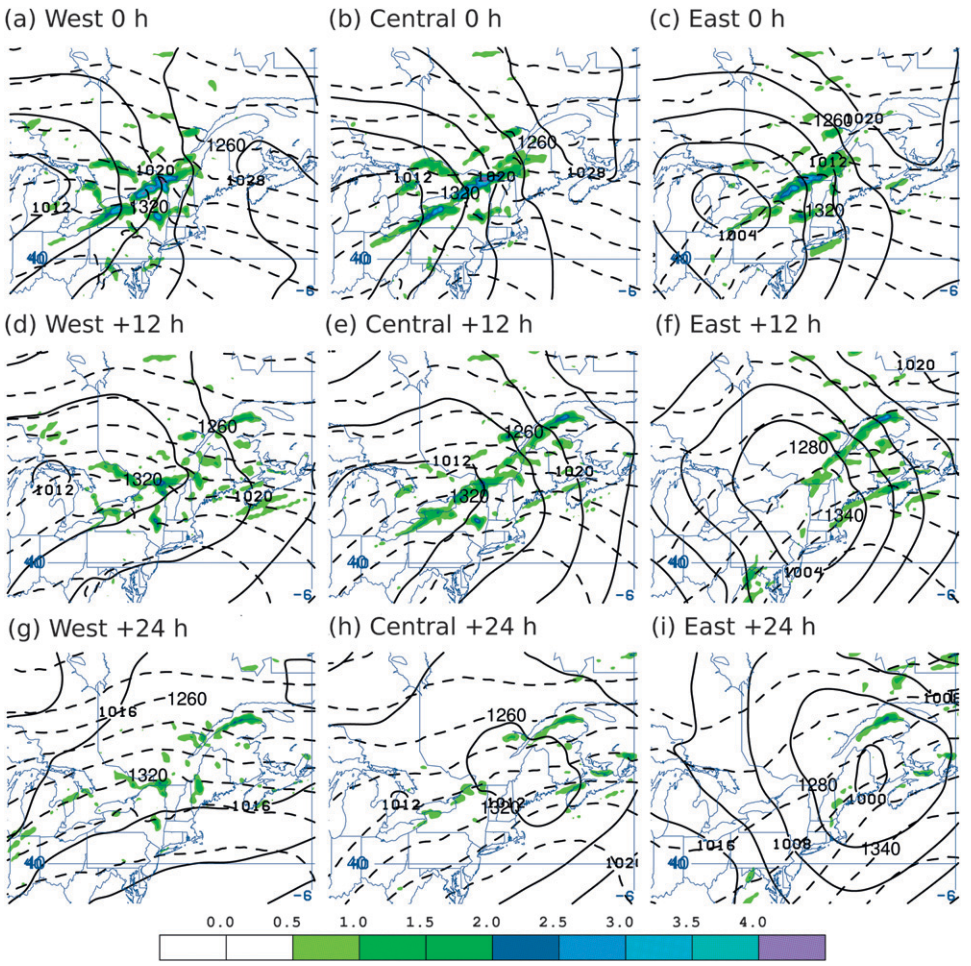

FIG. 12. Composite 1000–850-hPa thickness (dashed, 20-m contour interval), SLP (solid, 4-hPa contour interval), and layer-mean 1000–850-hPa frontogenesis [shaded, K (100 km)$^{-1}$ (3 h)$^{-1}$] at $t = 0$, +12, and +24 h for (a),(d),(g) west, (b),(e),(h) central, and (c),(f),(i) east events.

including Montreal (CYUL). Severe events can have a devastating effect on people, property, and commerce. For this reason, gaining insight into Quebec freezing rain events is important not only to the forecasters responsible for making freezing rain predictions, but to the industries and citizens affected by severe icing. This paper presents a synoptic-scale analysis of long-duration freezing rain events in Montreal for the time period 1979–2008. Out of 163 synoptically independent freezing rain events, 46 are categorized as long duration, with ≥6 hours of freezing rain per event. The long-duration events are further partitioned into three types—west ($n = 10$), central ($n = 16$), and east ($n = 20$)—based on the location and tilt of the 500-hPa trough axis.

West events are characterized by a positively tilted, long-wavelength upper-level trough over the western third of North America. The long upper-level wavelength of west events corresponds to a slower eastward movement of the trough and associated surface features. As a result, freezing rain at CYUL tends to last longer for west events. The freezing rain event with the longest duration in Montreal for this time period, the 1998 Ice Storm, is classified as a west event. The west composite of 1000–500-hPa thickness shows statistically significant warm anomalies over the central United States 48 h before the onset of freezing rain. This strong WAA acts to build the long-wave ridge over eastern Canada. A comparison of the 500-hPa heights for all three types indicates that west events display the highest 500-hPa heights at CYUL at the time of freezing rain onset. The strong WAA and subsequent ridge building likely slow the wave train's eastward progress, contributing to the prolonged duration of west events.

The west composite of 1000–500-hPa thickness also displays strong CAA and impressive cold anomalies over

TABLE 2. Total (solid, liquid, and freezing) precipitation accumulations and precipitation rates for events in each synoptic type. Values are calculated using Environment Canada 6-hourly total precipitation accumulation for CYUL.

Variable	West	Central	East
Total number of events (n)	10	16	20
Median total event precipitation (mm)	21.1	22.5	23.7
Median duration (h)	39	30	30
Median event precipitation rate (10^{-1} mm h^{-1})	5.4	7.3	7.8
Maximum event precipitation rate (10^{-1} mm h^{-1})	10.7	11.1	17.5

Quebec, Newfoundland, and Labrador in the 48 h leading up to freezing rain onset. This means that more cold air is available to sustain the low-level temperature inversion within the SLRV, as long as the winds within the valley are northeasterly.

The dominant surface feature associated with west events is a strong high pressure system to the east of CYUL. This usually takes the form of a strong Atlantic anticyclone, combined with a secondary anticyclone or surface ridge over eastern Quebec or the Maritime Provinces. In all west events, an inverted surface trough extends from Texas toward the Great Lakes, and the resulting geostrophic flow directs warm, moist air up from the Gulf of Mexico. The area of strong surface geostrophic frontogenesis over Quebec, with cold arctic air to the northeast and warm Gulf air to the southwest, strengthens the temperature gradient perpendicular to the axis of the SLRV. This broad-scale frontogenesis is enhanced by the topography of the SLRV, as the cold air is channeled northeasterly down the valley under the warm southerlies. This valley-enhanced frontogenesis can sustain freezing rain events for long periods of time, such as in the 1998 Ice Storm (Roebber and Gyakum 2003). West events are usually longer in duration, but precipitation rates are weaker, owing to weaker upper-level forcing for ascent.

Central events are characterized by an upper-level pattern similar to west events, but with the long-wave trough axis located farther to the east. For this reason, central events tend to be shorter in duration than west events, but longer in duration than east events. Although central events display the most within-type variability, the dominant surface pattern is a cyclone–anticyclone couplet. Similar to west events, central events are characterized by a surface trough of low pressure extending northward into the Great Lakes region from the Gulf of Mexico. However, the low pressure centers in central events tend to be deeper and more well defined (i.e., most central events have low pressure centers with closed circulation).

East events are characterized by a negatively tilted, short-wave upper-level trough over the Great Lakes region. The upper-level trough and associated surface features tend to move through CYUL more quickly than west or central events. Unlike west and central events, anomalously cold 1000–500-hPa thicknesses in northern Quebec and Labrador do not appear to be necessary for the production of freezing rain. A weaker cold pool of air suggests a weaker low-level temperature inversion, given northeasterly channeled winds within the SLRV.

East events represent a more classic freezing rain setup, where freezing rain occurs north of the warm or occluded front in a midlatitude cyclone as a result of WAA occurring above a shallow dome of cold air. Therefore, the dominant surface feature associated with east events is a fast-moving, well-defined midlatitude cyclone. Typically, the duration of freezing rain associated with this type of weather pattern is limited, since the frontal passage (warm or occluded) will change the precipitation to rain or snow. However, at CYUL, long-duration freezing rain events associated with a midlatitude cyclone appear to be prolonged by the topographic effects of the SLRV. As in the west and central cases, northeasterly channeling of the surface winds helps to sustain the temperature inversion, prolonging the duration of freezing rain. Although east events have, on average, the shortest duration of freezing rain, the precipitation intensity can be considerable (Table 2), with stronger QG forcing for ascent.

In each composite, cold-air advection at the surface is provided by the pressure-driven channeling of northeasterly surface winds. To produce pressure-driven channeling, a PGF must be aligned along the SLRV, as a result of either an anticyclone to the northeast, a cyclone to the southwest, or a cyclone–anticyclone couplet. Forecasters should note that in certain situations, even though there may be a strong PGF aligned with the SLRV, southerly channeling from the Lake Champlain Valley (LCV) may overpower the northeasterly channeled winds at CYUL (Razy et al. 2012). Southerly winds in these situations are associated with WAA at the surface, and will act to destroy the low-level temperature inversion. In the LCV, southerly channeling is often a result of forced or pressure-driven channeling or a combination of both (Carrera et al. 2009; Razy et al. 2012). As an added complication, the SLP fields that produce southeasterly winds at CYUL are often very similar to those that produce northeasterly winds (Razy et al. 2012). Forecasters should pay close attention to the surface winds in the hours leading up to and during freezing rain events at CYUL.

TABLE 3. Synoptic characteristics associated with each type of freezing rain event.

	500-hPa height	SLP	1000–500-hPa thickness
West ($n = 10$)	Positively tilted long-wave trough over the west coast of North America	Atlantic anticyclone, secondary anticyclone or ridge over Quebec and the Maritime Provinces	CAA and anomalously cold thicknesses over Quebec 48 h before onset of freezing rain
		Inverted trough extending from Texas to the Great Lakes region	WAA and anomalously warm thicknesses over the central United States 48 h before onset of freezing rain
		Southwesterly geostrophic wind	
Central ($n = 16$)	Positively tilted long-wave trough east of the Front Range of the Rockies, with a ridge building over the West Coast	Anticyclone over Quebec or the Maritime Provinces	CAA and anomalously cold thicknesses over Quebec 48 h before onset of freezing rain
		Low pressure (closed circulation) extending from the Gulf of Mexico to the Great Lakes region	WAA and anomalously warm thicknesses over the Great Lakes region 24 h before freezing rain onset
		Southerly geostrophic wind	
East ($n = 20$)	Negatively or neutrally tilted long-wave trough east of 95°W	Strong, well-defined surface cyclone centered over the Great Lakes region	Lack of strong CAA before freezing rain onset
		Lack of strong downstream anticyclone	WAA and anomalously warm thicknesses over southern Ontario 24 h before freezing rain onset

Since the location and severity of freezing rain remains difficult to accurately predict, it is our hope that the synoptic-scale structures presented in this study will benefit the local forecaster. For this reason, a quick reference guide to the important conclusions highlighted in this paper is provided in Table 3.

Since this study focuses on only one location, more work is needed to assess the spatial extent of freezing rain within the SLRV and the surrounding area. A comparison of the events presented here to other events within the SLRV, such as Quebec City (CYQB), would provide further insight into the precipitation structures and severity of each type, as well as the role of local topography and wind channeling.

Additionally, more work is needed to assess the predictability of each synoptic type. It can be suggested that since long-wave features tend to move more slowly than short-wave features, long-duration west events may have an inherently higher predictability at days 3–5 than central or east events; however, further work is needed to quantify this. Also, since sustained freezing rain at CYUL is heavily reliant on the topography of the St. Lawrence River Valley (Roebber and Gyakum 2003), the resolution of any model used, whether for operational or reanalysis purposes, is an important factor. In the future, it is hoped that the long-duration events documented in this study can be replicated using high-resolution mesoscale modeling.

Finally, we hope that this study will also provide the foundation necessary to assess the future risk of freezing rain in Quebec, relative to our changing climate. A synoptic-scale understanding of freezing rain events will be essential to placing future climate scenarios in an appropriate physical context.

Acknowledgments. This work was supported, in part, by an Ouranos Consortium research grant, by the Mathematics of Information Technology and Complex Systems (MITACS), and by a Natural Sciences and Engineering Research Council (NSERC) Discovery Grant. The authors thank NCEP for access to the NARR dataset and Environment Canada for access to their climate information databases. The authors would also like to acknowledge the DAI Team for providing the precipitation data and technical support. The DAI web portal (http://loki.qc.ec.gc.ca/DAI/) is made possible through collaboration among the Global Environmental and Climate Change Centre (GEC3), the Adaptation and Impacts Research Division (AIRD) of Environment Canada, and the Drought Research Initiative (DRI). The Ouranos Consortium (in Quebec) provides access of the Canadian Regional Climate Model (CRCM). Finally, we would like to acknowledge Dr. Paul Roebber and two anonymous reviewers for their extremely helpful reviews of this manuscript.

APPENDIX

List of Long-Duration Events

TABLE A1. List of Montreal long-duration freezing rain events, 1979–2008.

Onset time	Hours of freezing rain	Classification
0600 UTC 14 Jan 1979	10	East
0900 UTC 28 Nov 1980	9	East
0400 UTC 28 Nov 1982	11	West
0600 UTC 24 Dec 1982	14	West
1800 UTC 23 Jan 1983	14	East
1100 UTC 7 Mar 1983	10	Central
1700 UTC 21 Mar 1983	9	East
0000 UTC 14 Dec 1983	22	Central
0400 UTC 19 Mar 1984	10	Central
1700 UTC 28 Dec 1984	19	West
2200 UTC 24 Feb 1985	6	East
1500 UTC 10 Mar 1986	18	East
0600 UTC 25 Dec 1986	8	Central
2000 UTC 4 Mar 1989	20	Central
0700 UTC 28 Nov 1989	9	Central
0700 UTC 16 Feb 1990	9	Central
0800 UTC 4 Dec 1990	7	East
2300 UTC 21 Dec 1990	9	West
1500 UTC 3 Mar 1991	26	East
1700 UTC 3 Dec 1991	7	East
1000 UTC 11 Mar 1992	9	East
2300 UTC 29 Dec 1992	19	West
2100 UTC 3 Jan 1993	7	West
0700 UTC 28 Jan 1994	7	Central
0400 UTC 13 Jan 1995	7	Central
0300 UTC 5 Jan 1997	9	East
0000 UTC 22 Feb 1997	13	Central
0600 UTC 5 Jan 1998	62	West
0200 UTC 6 Dec 1998	7	West
0100 UTC 23 Jan 1999	6	Central
1200 UTC 2 Feb 1999	6	East
1200 UTC 9 Feb 2001	10	Central
1500 UTC 29 Nov 2001	14	Central
2000 UTC 23 Dec 2001	8	East
0800 UTC 23 Feb 2003	6	East
1600 UTC 5 Apr 2003	12	West
2000 UTC 4 Nov 2003	7	West
0300 UTC 17 Dec 2003	6	East
2100 UTC 7 Dec 2004	7	East
0300 UTC 28 Nov 2005	8	Central
1000 UTC 26 Dec 2005	20	East
0200 UTC 18 Jan 2006	8	East
1100 UTC 30 Jan 2006	7	East
1700 UTC 1 Dec 2006	9	East
0200 UTC 10 Dec 2008	9	Central
1300 UTC 27 Dec 2008	6	Central

REFERENCES

Amante, C., and B. W. Eakins, 2009: ETOPO1 1 arc-minute global relief model: Procedures, data sources and analysis. NOAA Tech. Memo. NESDIS NGDC-24, 9 pp.

Bernstein, B. C., T. A. Omeron, M. K. Politovich, and F. McDonough, 1998: Surface weather features associated with freezing precipitation and severe in-flight icing. *Atmos. Res.,* **46,** 57–73.

Bluestein, H. B., 1992: *Principles of Kinematics and Dynamics*. Vol. 1, *Synoptic–Dynamic Meteorology in Midlatitudes,* Oxford University Press, 431 pp.

Bocchieri, J. R., 1980: The objective use of upper air soundings to specify precipitation type. *Mon. Wea. Rev.,* **108,** 596–603.

Bourgouin, P., 2000: A method to determine precipitation types. *Wea. Forecasting,* **15,** 583–592.

Carrera, M. L., J. R. Gyakum, and C. A. Lin, 2009: Observational study of wind channeling within the St. Lawrence River Valley. *J. Appl. Meteor. Climatol.,* **48,** 2341–2361.

Cheng, C. S., H. Auld, G. Li, J. Klaassen, B. Tugwood, and Q. Li, 2004: An automated synoptic typing procedure to predict freezing rain: An application to Ottawa, Ontario, Canada. *Wea. Forecasting,* **19,** 751–768.

Cortinas, J. V., 2000: A climatology of freezing rain in the Great Lakes region of North America. *Mon. Wea. Rev.,* **128,** 3574–3588.

——, B. C. Bernstein, C. C. Robbins, and J. W. Strapp, 2004: An analysis of freezing rain, freezing drizzle, and ice pellets across the United States and Canada. *Wea. Forecasting,* **19,** 377–390.

Czys, R. R., R. W. Scott, K. C. Tang, R. W. Przybylinski, and M. E. Sabones, 1996: A physically based, nondimensional parameter for discriminating between locations of freezing rain and ice pellets. *Wea. Forecasting,* **11,** 591–598.

DAI, cited 2010: Data Access Integration portal. [Available online at http://loki.ouranos.ca/DAI/.]

Dore, M. H. I., 2003: Forecasting the conditional probabilities of natural disasters in Canada as a guide for disaster preparedness. *Nat. Hazards,* **28,** 249–269.

Forbes, G. S., R. A. Anthes, and D. W. Thomson, 1987: Synoptic and mesoscale aspects of an Appalachian ice storm associated with cold air damming. *Mon. Wea. Rev.,* **115,** 564–591.

Gyakum, J. R., and P. J. Roebber, 2001: The 1998 ice storm—Analysis of a planetary-scale event. *Mon. Wea. Rev.,* **129,** 2983–2997.

Henson, W., and R. Stewart, 2007: Severity and return periods of icing events in the Montreal area. *Atmos. Res.,* **84,** 242–249.

——, ——, and B. Kochtubajda, 2007: On the precipitation and related features of the 1998 ice storm in the Montreal area. *Atmos. Res.,* **83,** 36–54.

Higuchi, K., C. W. Yuen, and A. Shabbar, 2000: Ice storm '98 in south-central Canada and northeastern United States: A climatological perspective. *Theor. Appl. Climatol.,* **66,** 61–79.

Hoskins, B. J., I. Draghici, and H. C. Davies, 1978: A new look at the ω-equation. *Quart. J. Roy. Meteor. Soc.,* **104,** 31–38.

Huffman, G. J., and G. A. Norman, 1988: The supercooled warm rain process and the specification of freezing precipitation. *Mon. Wea. Rev.,* **116,** 2172–2182.

Kain, J. S., S. M. Goss, and M. E. Baldwin, 2000: The melting effect as a factor in precipitation-type forecasting. *Wea. Forecasting,* **15,** 700–714.

Koch, S., M. Desjardins, and P. Kocin, 1983: An interactive Barnes objective map analysis scheme for use with satellite and conventional data. *J. Appl. Meteor.,* **22,** 1487–1503.

Lackmann, G. M., K. Keeter, L. G. Lee, and M. B. Ek, 2002: Model representation of freezing and melting precipitation: Implications for winter weather forecasting. *Wea. Forecasting,* **17,** 1016–1033.

Laflamme, J. N., and G. Periard, 1998: The climate of freezing rain over the province of Québec in Canada: A preliminary analysis. *Atmos. Res.,* **46,** 99–111.

MacKay, G. A., and H. A. Thompson, 1969: Estimating the hazard of ice accretion in Canada from climatological data. *J. Appl. Meteor.,* **8,** 927–935.

Martner, B. E., J. B. Snider, R. J. Zamora, G. P. Byrd, T. A. Niziol, and P. I. Joe, 1993: A remote sensing view of a freezing rainstorm. *Mon. Wea. Rev.,* **121,** 2562–2577.

Mesinger, F., and Coauthors, 2006: North American Regional Reanalysis. *Bull. Amer. Meteor. Soc.,* **87,** 343–360.

Milton, J., and A. Bourque, 1999: A climatological account of the January 1998 ice storm in Quebec. Environment Canada Tech. Rep. CES-Q99-01, 87 pp.

Rauber, R. M., M. K. Ramamurthy, and A. Tokay, 1994: Synoptic and mesoscale structure of a severe freezing rain event: The St. Valentine's Day ice storm. *Wea. Forecasting,* **9,** 183–208.

——, L. S. Olthoff, M. K. Ramamurthy, and K. E. Kunkel, 2000: The relative importance of warm rain and melting processes in freezing rain precipitation events. *J. Appl. Meteor.,* **39,** 1185–1195.

——, ——, D. Miller, and K. E. Kunkel, 2001: A synoptic weather pattern and sounding-based climatology of freezing precipitation in the United States east of the Rocky Mountains. *J. Appl. Meteor.,* **40,** 1724–1747.

Razy, A., S. M. Milrad, E. H. Atallah, and J. R. Gyakum, 2012: Synoptic-scale environments conducive to orographic impacts on cold-season surface wind regimes at Montreal, Quebec. *J. Appl. Meteor. Climatol.,* **51,** 598–616.

Regan, M., 1998: Canadian ice storm 1998. *WMO Bull.,* **47,** 250–256.

Roebber, P. J., and J. R. Gyakum, 2003: Orographic influences on the mesoscale structure of the 1998 ice storm. *Mon. Wea. Rev.,* **131,** 27–50.

Statistics Canada, 1998: The St. Lawrence River Valley 1998 ice storm: Maps and facts. Statistics Canada Rep. 16F0021XIB1998001, 17 pp.

Stewart, R. E., 1985: Precipitation types in winter storms. *Pure Appl. Geophys.,* **123,** 597–609.

Stuart, R. A., and G. A. Isaac, 1999: Freezing precipitation in Canada. *Atmos.–Ocean,* **37,** 87–102.

Wilks, D. S., 2006: *Statistical Methods in the Atmospheric Sciences*. 2nd ed. Academic Press, 630 pp.